Volcanic hazard exacerbated by global warming–driven increase in heavy rainfall

Jamie I. Farquharson[1], Falk Amelung[1]

[1] Rosenstiel School of Marine and Atmospheric Science, University of Miami, Miami, FL, USA

Corresponding author: jifarq89@googlemail.com

Abstract

Heavy rainfall drives a range of eruptive and noneruptive volcanic hazards; over the Holocene, the incidence of many such hazards has increased due to rapid climate change. Here we show that extreme heavy rainfall is projected to increase with continued global warming throughout the 21st century in most subaerial volcanic regions, dramatically increasing the potential for rainfall-induced volcanic hazards. This result is based on a comparative analysis of nine general circulation models, and is prevalent across a wide range of spatial scales, from countries and volcanic arcs down to individual volcanic systems. Our results suggest that if global warming continues unchecked, the incidence of primary and secondary rainfall-related volcanic activity will increase at more than 700 volcanoes around the globe. Improved coupling between scientific observations—in particular, of local and regional precipitation—and policy decisions, may go some way towards mitigating the increased risk throughout the next 80 years.

Climate change and volcanism

The role of Earth's subaerial volcanism in driving past climate changes has been substantial[1]—due in large part to the radiative and chemical effects of erupted gases and aerosols[2]—and it is anticipated to drive further variability in the future[3,4]. In turn, variations in climate have also been posited to drive volcanic activity[5–7]. Mechanisms such as the isostatic unloading of the crust due to warming-induced glacial retreat and ice cap melt[8,9] or crustal stress changes generated by changing sea levels[10] have been proposed to promote volcanic activity over a range of spatio-temporal scales. Over the last 30 ka, changes in climate have driven an increase in massive volcanic collapses, partly in response to increased humidity and rainfall[11]. An uptick in rainfall-driven volcanic hazards has been proposed for many volcanic regions as global climate continues to warm throughout the Anthropocene; in particular, in unglaciated highrelief volcanic environments[6]: an observable rate change in hazardous geological phenomena that may already be underway[12].

Extreme or seasonal rainfall has been identified as a trigger mechanism for primary volcanic activity—discrete eruptions of lava, tephra, and gases—at multiple volcanoes. Examples include rainfall-triggered explosions at Mount St Helens (USA), Gunung Merapi (Indonesia), and Las Pilas (Nicaragua)[13–15]. Coupling between extreme rainfall events and dome collapse has also frequently been noted[16–20], with heavy rainfall also being linked to the generation of pyroclastic density currents[19]. More recently, a link between extreme rainfall, pore fluid changes at depth, and magma propagation has been proposedf[21]. Rainfall-triggered volcanism is often violently explosive[13], and multiple direct fatalities have been recorded as a result, including at Karkar[22], Guagua Pichincha[23], and Karangetang[24] volcanoes (Papua New Guinea, Ecuador, and Indonesia, respectively). Many hazards associated with extreme precipitation events or prolonged rainfall are heightened in volcanic regions: not only do mountainous regions tend to modify and amplify precipitation[25], but they are often mantled by variably consolidated tephra deposits and other easily mobilised debris, and can be associated with large thermal gradients. Not only can these gradients drive explosive fuel-coolant interactions[26], but thermal atmospheric forcing due volcanic thermal anomalies can also increase precipitation above the threshold required to trigger hazards[27]. These factors promote a range of rainfall-related secondary volcanic hazards, including the remobilisation of volcanogenic deposits in the form of lahars[28–30] and the instigation of flank mass movement[31–34], a phenomenon that can in turn unload the magma chamber and promote explosive decompression or dyke initiation[35]. Volcanic slopes, typically with low cohesion and narrow grain-size distributions, may be particularly disposed to mass wasting events[34]. Further, A textual analysis of the Smithsonian's Global Volcanism Program Bulletin Reports—a multidecadal catalogue of reports of volcanic activity—reveals that extreme or heavy rainfall has been implicated in triggering or exacerbating hazards at at least 174 discrete volcanoes: around 13 % or 1 in every 7 of Earth's subaerial volcanic inventory (see **Methods**).

As the rate of global climate change continues to accelerate, it becomes ever more crucial to develop a comprehensive understanding of the manifold interactions and feedbacks between the atmosphere, cryosphere, and solid Earth: complexly interconnected components of the Earth system. Here we focus on the role of heavy rainfall in volcanic environments, and the evolution of rainfall rates over a multi-decadal timeframe induced by the ongoing rapid changes in global climate. A key problem with identifying volcanic regions at increasing risk has been the inherent uncertainty of climate modelling[6]. While there is broad consensus as to the direction of mean global precipitation change[36,37], global climate models (general circulation models: GCMs)—even when initiated with the same parameters—do not show general concurrence upon the magnitude or spatial distribution of precipitation change, and observations of global mean precipitation changes are at often odds with projected changes[38]. Consistently, however, these models project an increase in the intensity and frequency of heavy precipitation—that is, extreme precipitation events—both on global and regional scales[39]. Fischer et al.[40] and Pfahl et al.[41] demonstrate that global climate models tend to concur when considering future heavy precipitation. In particular, those authors found that most models tested in their analysis agreed on the sign of change of the diurnal maximum precipitation over time at any given location.

In this contribution, we analyse a suite of numerical global climate models to assess which of Earth's subaerial volcanoes are projected to experience increases or decreases in extreme rainfall, revealing several volcanic systems which we estimate will become more susceptible to rainfall-induced hazards over the next 80 years. In particular we focus on the forced model response (FMR), the percentage change of heavy precipitation for a given unit of global warming, which serves as a proxy for the likelihood of extreme rainfall events, calculated from nine Coupled Model Intercomparison Project Phase 5 (CMIP5) general circulation models (**Methods**).

Climate models agree on the direction of heavy precipitation change with global warming

Calculate forced model responses from the individual CMIP5 general circulation models are shown in **Figure 1**, presented in % C^{-1} as the gradient of a regression between monthly heavy precipitation change RX and global mean temperature $\langle T \rangle$. There is qualitative agreement in many areas across models (**Figure 1**): less extreme rainfall is forecast by most models for the majority of Australia, parts of Saharan and southern Africa, and Central America, for example, whereas large portions of North America, Eurasia, East Africa, and the Polar regions are projected to experience an increase in extreme precipitation with continued global warming. This is emphasised by mean response of all models resized onto a common grid (**Figure 2a**). The areas where fewer than seven of nine models agree on the sign of FMR are shaded. The area over which at least seven of nine models concur accounts for 73.45 % of the globe, in line with previous multi-model studies[40,41], despite the fact that the cited studies examine models at a daily resolution over longer timescales (including historical simulations) and analyse more models (15 and 22, respectively). As well as the proportion of model agreement, we highlight that the areas of agreement are qualitatively similar to those of refs. [40,41]. In a volcanic context, regions where extreme rainfall is projected to increase account for large portions of each of the continental volcanic arcs (the Cascades, the Alaskan Peninsula and Aleutian Range, Kamchatka, and Northern and Central Andes), parts of the the Mediterranean and East African Rift system, and throughout the Sunda, Philippine, Ryuku, Japan, Kuril, Aleutian and West Indies island arcs. Smaller subtropical island arcs, including the Bismarck Archipelago are also encompassed. On the other hand, models tend to agree that extreme rainfall will decrease in parts of the Southern Andean Volcanic Zone and Rangitāhua (the Kermadec Islands), for example.

Of the 1296 Holocene-active subaerial volcanic systems included in the initial dataset, 768 (59 %) are situated in regions with a positive FMR (i.e. regions that are forecast to experience more extreme rainfall over the next 80 years) across the majority of GCMs (**Figure 2b**). 244 of these (19 % of the initial dataset) have a mean (averaged over all models) FMR ≥5 % C^{-1}. Nineteen volcanoes (1.5 %) exhibit a mean FMR ≥20 % C^{-1}, all of which are located in the Galápagos, the East African Rift, and Papua New Guinea, between 3.125°S and 25.000°N. Highlighted in **Figure 2b**, only 112 volcanoes (9 %) are located in regions anticipated to experience less extreme rainfall, with the remaining 416 (32 %) being associated with an ambiguous FMR (where fewer than 7 of the 9 models agreed with the sign of heavy precipitation change). The aggregate FMR distribution of each of the models is approximately symmetrical around a median of 3.2 % C^{-1}, indicating that the majority of the globe is projected to experience an increase in extreme rainfall. When we consider only those grid cells containing active volcanic systems (**Figure 2c**), we observe a lognormal distribution of volcanoes with positive FMR, with a mean value of ~4.5 % C^{-1} and a long tail on the positive side: the substantive majority of Earth's subaerial volcanic systems will be subject to more extreme rainfall with every increment of global warming over the remainder of the 21st century.

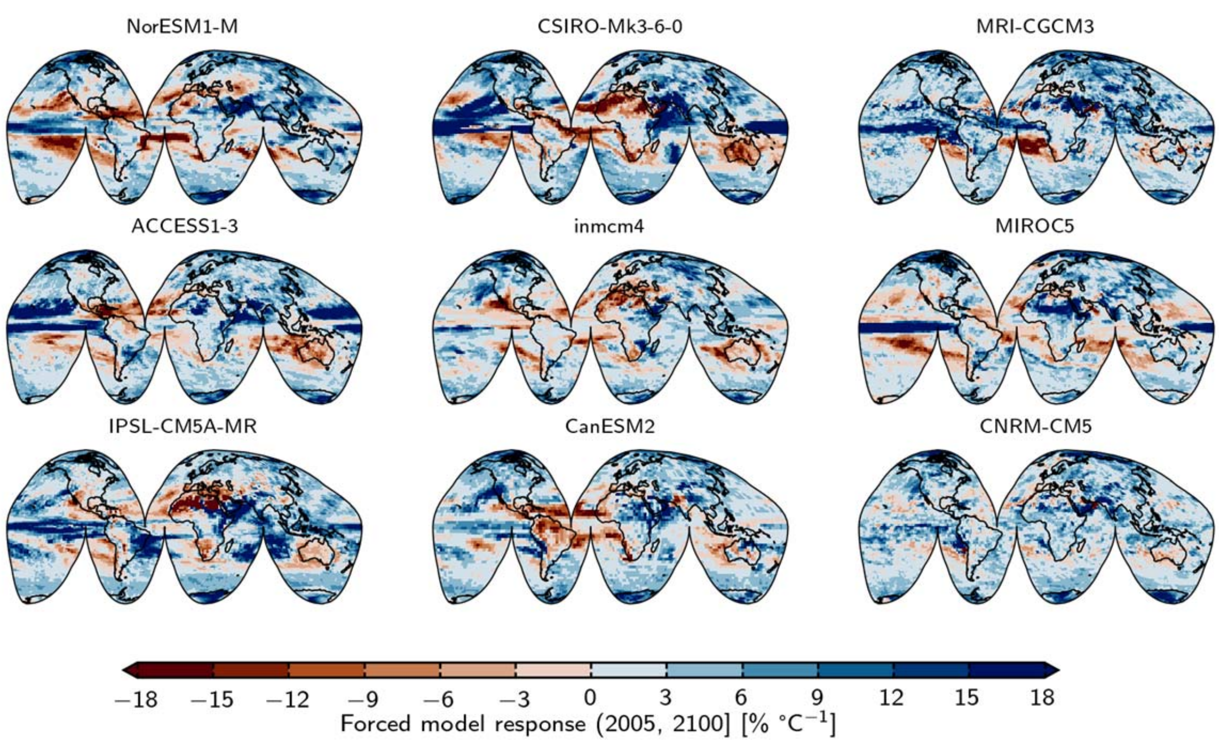

Figure 1 | Forced model response for all compared models. GCM codes (as listed in Table 1, **Methods**) are shown above the corresponding map. Forced model response (FMR) as RX versus $\langle T \rangle$ over the timeframe from 2005 or 2006 to 2100, normalised to 2006. Blue tones represent an increase in extreme rainfall with increased global warming, red tones represent a decrease.

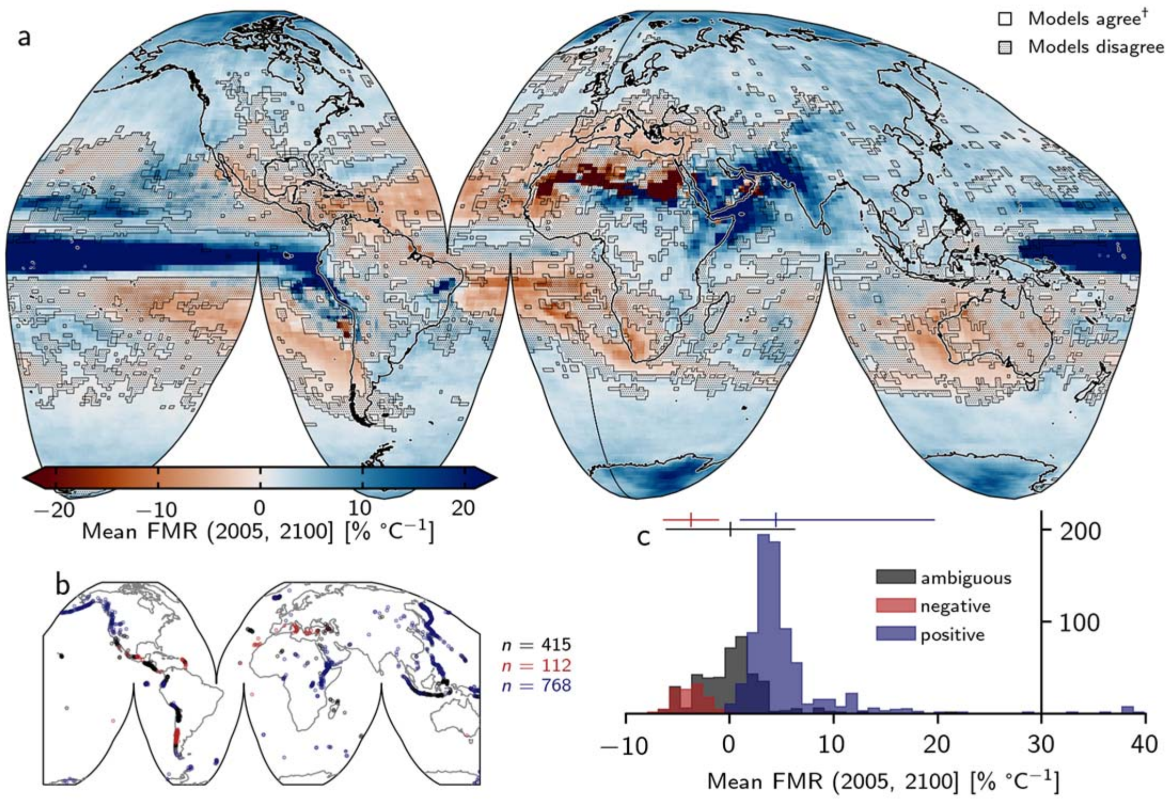

Figure 2 | Breakdown of mean forced model response. a Global mean forced model response (FMR) calculated from all models. Shaded area indicates those regions where fewer than seven of nine models agreed on the sign of change (26.55 %). †at least seven of nine models agree on the sign of change. **b** Subaerial volcano geolocations separated according to whether models agree on a decrease in heavy precipitation with increased warming (red: "negative"; n = 112); the precipitation response is ambiguous due to lack of model agreement (black: "ambiguous"; n = 415); models agree on an increase in heavy precipitation with increased warming (blue: "positive"; n = 768). n indicates the number of discrete Holocene-active volcanic systems in each category. **c** Histogram of mean FMR for each group of volcanoes (as in **b**). Mean and two standard deviation range are indicated by the vertical and horizontal lines, respectively (**Methods**).

Models project an increase in heavy precipitation for most or all volcanic regions

The GVP subdivides Earth's volcanoes into 19 discrete regions, which are further subdivided into 101 subregions. Extracting areal averages of these volcanic regions (those grid cells containing at least one Holocene-active volcano: discrete coloured rectilinear polygons in **Figure 3a**), we calculate the linear regression–based gradient of change in heavy precipitation versus global warming.

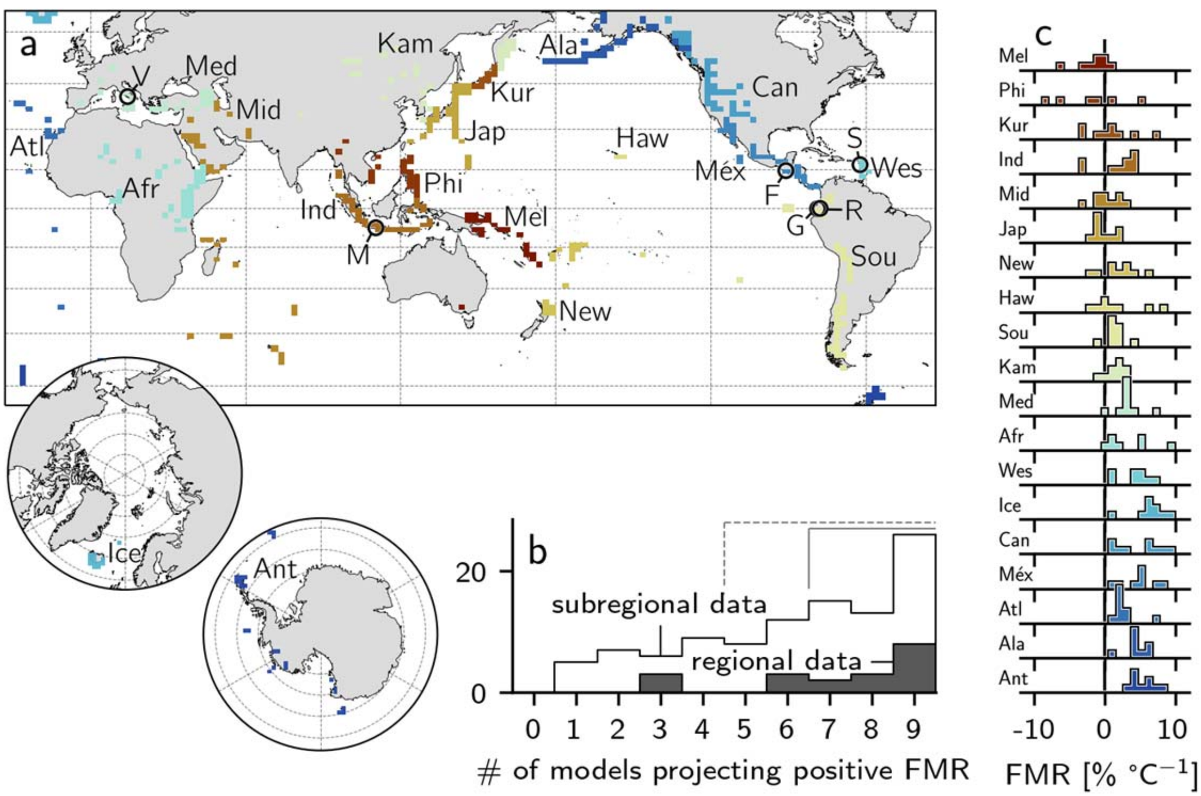

Figure 3| Regional and sub-regional spatial averages. a Map indicating the noncontiguous spatial extent over which regional data are averaged. Circle markers indicate individual volcanoes shown in **Figure 4**. V = Vesuvius, M = Merapi, F = Fuego, R = Reventador, G = Guagua Pichincha, S = Soufrière Hills Volcano. [Inset] polar regions. Regions are represented by discrete coloured rectilinear polygons. Ant = Antarctica; Atl = Atlantic Ocean; Sou = South America; Ala = Alaska; Kur = Kuril Islands; Ind = Indonesia; Mid = Middle East and Indian Ocean; Phi = Philippines and SE Asia; Méx = México and Central America; Jap = Japan, Taiwan, and Marianas; Kam = Kamchatka and Mainland Asia; Med = Mediterranean and Western Asia; New = New Zealand to Fiji; Haw = Hawai`i and Pacific Ocean; Ice = Iceland and Arctic Ocean; Afr =

Africa and Red Sea; Wes = West Indies; Mel = Melanesia and Australia; Can = Canada and Western USA. **b** Bar chart of the number of regions and subregions where x number of models project a spatially averaged forced model response (FMR) > 0 (i.e. a concomitant increase in heavy precipitation and global mean temperature). Dashed bracket indicates the majority of models, solid bracket indicates 7 or more out of 9 models. **c** Inter-model distributions of calculated FMR for each region.

For each region, **Figure 3b** indicates the distribution of models (out of a maximum of nine) that project a positive FMR: a concomitant increase in heavy rainfall with global warming. For the vast majority of volcanic regions (16/19: 84 %), most models project positive FMR. Of these, 13 (64 %) exhibit agreement across at least seven models, and for 8 regions (Antarctica; Atlantic Ocean; Alaska; Africa and Red Sea; México and Central America; Iceland and Arctic Ocean; West Indies; Canada and Western USA) all models forecast a positive FMR (42 % of all regions). There are zero volcanic regions for which at least seven of nine models project a negative FMR. This trend is echoed at the sub-regional scale (**Figure 3b**): the majority of models forecast positive FMR for 74 of 101 subregions (73 %), and of these, 54 (53 %) exhibit agreement between at least seven models. There are no volcanic regions for which more than seven models project a negative FMR. both the region and subregion scale, the observed distributions are statistically nonuniform, characterised by $\mathrm{CDF}(\chi^2) \ll 0.01$. **Figure 3c** shows the distribution of calculated gradients across models for each region. Note that majority-positive FMR distributions (e.g. Antarctica, Alaska, Atlantic Ocean, Mediterranean and Western Asia, Kamchatka and Mainland Asia: **Figure 3c**) tend to be relatively tightly clustered, whereas for those regions where FMR is predominantly negative or ambiguous (e.g. Philippines, Kuril Islands, Hawai`i and Pacific Ocean: **Figure 3c**), the distribution tends to be broader. This emphasises the fact that when we observe reasonable inter-model concurrence in any given region, the result is usually that heavy rainfall is set to increase over the next 80 years.

Illustrative examples of regionally averaged climate projections are given in Figure 4a-f, highlighted here due to the demonstrable risk of rainfall-induced hazard therein (data for all regions and subregions are provided as **supplementary material 1**). The Atlantic ocean volcanic region (**Fig. 3a**, **Fig. 4a**) largely comprises island volcanoes characterised by a history of catastrophic collapse—including Tristan de Cunha, El Hierro, and Tenerife—a potential tsunamigenic hazard facilitated by wet climates[42]. The Canada and Western USA volcanic region (**Fig. 3a**, **Fig. 4b**) is predominantly composed of stratovolcanoes in the Cascade Range. The incidence of sector collapse at several Cascadian volcanoes (including Mount St Helens, Mt Adams, and Mt Baker) has been proposed to be triggered or exacerbated by historical climate change, including the attendant increase in humidity and rainfall[11]. Numerous volcanoes in the Cascade

Range currently present a significant lahar threat to major population centres[43], with several exhibiting flank segments in excess of 20° slope pitch (calculated from ref.[44]). Notably, direct evidence of rainfall-triggered explosive activity has been reported for Mount St Helens[13]am. The Alaska region (**Fig. 3a**, **Fig. 4c**)—including the Alaskan Peninsula, Aleutian Range, and Aleutian island arc—hosts volcanoes with the highest mean and partial flank inclines (in excess of 30 and 40°, respectively[44]). Holocene climate change has already been shown to have driven geologically recent volcanic sector collapse in parts of the Mediterranean and Western Asia region (**Fig. 3a**, **Fig. 4d**)[45], with these areas highlighted as becoming increasingly hazard-prone in the future[12]. The West Indies region (**Fig. 3a**, **Fig. 4e**) has similarly been highlighted[12], and hosts frequently active volcanoes such as Soufrière Hills where primary volcanic activity is observably triggered by heavy rainfall[16,19]. Finally, Indonesia (**Fig. 3a**, **Fig. 4f**)—the world's most volcanically active country and a volcanic region unto itself—is home to multiple volcanoes where explosive behaviour has been triggered by heavy rainfall. Notable examples of activity following prolonged or extreme rainfall include the unexpected onset of an eruption at Egon in 2004, explosions and dome instabilities at Lokon-Empung in 2002 and 2011, and the sudden and tragically fatal explosive activity at Karangetang in 2010 (see **supplementary material 2**).

Clearly, each of these regions appears particularly hazard-prone in terms of heavy rainfall–driven phenomena. Just as clearly, heavy rainfall is projected to increase in these regions by most or all climate models, thus heightening an already considerable threat to life, property, and infrastructure in the coming decades.

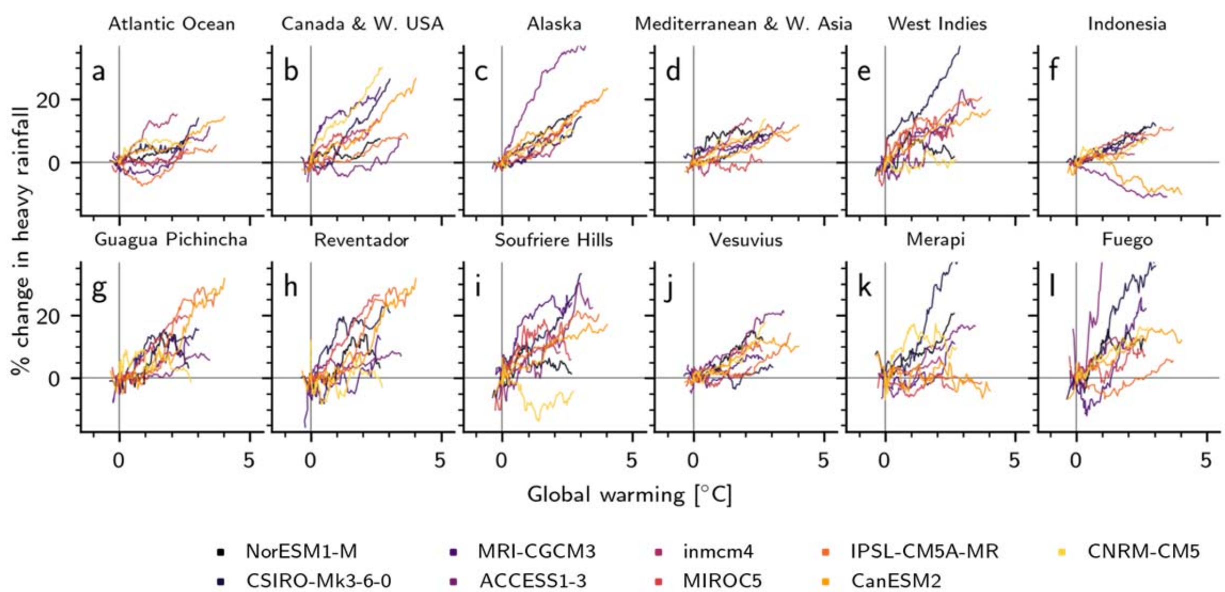

Figure 4 | Forced model responses at different spatial scales. a–f Percent change in modeled heavy rainfall per degree of global warming. Data are shown as a 30-yr rolling mean, normalised to January 2021. Dashed black lines are linear regression of response for each model. Data are areal averages (see **Figure 3** for areal extent of each region). **g–l** As **a–f**, for individual volcanic systems. Data correspond to the bounding pixel for each model (see **Methods**). Volcano locations are shown in **Figure 3**.

Climate change—induced hazards at individual volcanoes

Figure 4g-l presents the forced model responses at the scale of individual volcanic systems: Guagua Pichincha and Reventador, Ecuador; Soufrière Hills Volcano, Montserrat; Vesuvius, Italy; Gunung Merapi, Indonesia; and Fuego (Chi Q'aq'), Guatemala. These six volcanoes are chosen due to particularities of their eruptive histories, each of which illustrates the potential for increased hazard in the face of increased heavy precipitation. At Guagua Pichincha (**Fig. 3a**, **Fig. 4g**), cycles of explosivity have been anecdotally attributed to the timing of the rainy season[23]. A violent explosive eruption in 1993, triggered by "abnormally high" rainfall, resulted in the death of two volcanologists. Reventador (**Fig. 3a**, **Fig. 4h**), one of the most active volcanoes in Ecuador, is situated in a cloud-forest region already characterised by extremely heavy rainfall. Combined with its steep slopes[44], these factors contribute to the generation of frequent, often destructive, lahars. An analysis of Reventador's historical eruption catalogue indicates a tendency towards erupting between December and May, when the volcano receives the majority of its annual rainfall. Soufrière Hills Volcano (**Fig. 3a**, **Fig. 4i**) is characterised by sensitivity to heavy rainfall: not only does lahar probability scale directly with rainfall intensity[46], but triggered primary volcanic activity has been reported frequently[16,18,19]. At Vesuvius (**Fig. 3a**, **Fig. 4j**), textural, geochemical, and anecdotal evidence of external water—possibly of meteoric origin—exists for several previous large eruptions[47,48]. As with Reventador, we note a significant tendency for large historic eruptions to occur between July and December (the wettest time of year). In 1998, a protracted period of extreme rainfall mobilised pyroclastic debris from Vesuvius and the Campi Flegrei systems and generated devastating debris flows, resulting in 160 fatalities with many more injured or displaced[49]. A statistical correlation between intense rainfall and explosive dome collapse has been reported at Gunung Merapi[14] (**Fig. 3a**, **Fig. 4k**). The risk of lahars at Merapi—invariably driven by rainfall[50]—is substantial, with lahar deposits covering an area of almost 300 km^2 in the region. Rainfall-triggered lahars at Merapi have been responsible for many deaths and the destruction of thousands of homes. Finally, at Fuego (**Fig. 3a**, **Fig. 4l**), heavy rainfall has been attributed to a host of eruptive and non-eruptive hazards, triggering plume emissions, seismic activity, and tilt changes[51], as well being directly related to frequently triggered lahars. With climate models almost exclusively projecting an increase in heavy precipitation with continued warming for each of these systems, it is highly probable that the already substantial risk to people, property, and infrastructure at these systems will be further amplified in the coming decades.

Perspectives

In summary, we find that the majority of Holocene-active subaerial volcanic systems (768 volcanoes: 59 %) are confidently projected to experience more extreme rainfall as global temperatures continue to rise. Moreover, in some volcanic areas, heavy precipitation is projected to increase by as much as 46 % relative to the 2006 value for every degree of warming experienced over the next 80 years. For another 32 % of volcanoes globally (in particular at mid-latitudes), there is not sufficient inter-model consensus to confidently estimate whether rainfall will become more or less extreme in the future. Ultimately, these results point to significant attendant implications for rainfall-related hazards at most of Earth's subaerial volcanic systems.

Multidecadal catalogues of reports of volcanic activity reveal that rainfall has historically triggered, facilitated, or worsened primary volcanic activity or secondary hazards at over 170 subaerial volcanoes; a strong reminder that the influence of the hydrological cycle in volcanic systems can be substantial. This link emphasises the importance of considering rainfall in the development of hazard mitigation strategies[19,46,52], and also underscores the importance of developing novel instrumental monitoring systems[53,54]. The incorporation of meteorological data into volcano monitoring systems has seen some limited adoption[55]; nevertheless, meteorological data is far from being a standard monitoring tool.

While much previous emphasis has been placed on the effect of climate change on tropical volcanoes[56], we highlight that an increase in heavy precipitation is projected to occur with warming in many polar and temperate volcanic regions as well, including the Aleutian Arc, Western USA and Canada, and Antarctica and the South Sandwich Islands, as well as arid regions such as north Africa (**supplementary material 1**). In resolving cross-model agreement at regional and local scales relevant for volcanic hazard, we demonstrate an explicit, geographically widespread link between global warming scenarios and the potential for increased volcanic hazard. We have not accounted for the influence of global warming on the dynamics of eruption plumes[57], nor for the proposed orographic feedback between heated volcanic summits and precipitation[58] which may serve to further exacerbate the influence of rainfall in volcanic regions. We highlight that broader feedback mechanisms have also been proposed, including climate change—induced perturbations in crustal stress caused by ice-sheet and glacier wastage[56], changes to axial and spin-rate of the Earth and realignment of the geoid[5,59], and rising sea levels[60], each of which have the potential to trigger subaerial volcanism.

Methods

Textual analysis of Bulletin Reports

Geolocation data for Earth's subaerial volcanoes are obtained from the Smithsonian's Global Volcanism Program (GVP) databases[61] using the GVP webservices interface. We concentrate on volcanic systems active in the Holocene (discounting volcanoes defined as primarily submarine or subglacial): 1295 volcanoes. The prior association of any particular volcano with rainfall-related volcanic hazard was determined by programmatically querying the catalogue GVP Bulletin Reports for the (case-insensitive) string literals "lahar", "heavy rain", "rainfall-triggered", "rainfall-induced", and "extreme rainfall" (ignoring punctuation). The crawled reports were then manually parsed to identify volcanoes with previous evidence for volcanic hazard caused or exacerbated by rainfall, and to remove reports where rainfall was mention in non-hazard contexts (for example, reports on the effect of rainfall on monitoring equipment or the volcanic system that do not constitute a clear hazard, geographical background descriptions, or observational and logistical difficulties associated with inclement weather). The remaining catalogue refers specifically to hazards associated with heightened rainfall activity: steam explosions; the instigation of lahars and mudflows; column collapse and pyroclastic density current generation; landslides, rockfalls, and other mass wasting events; flooding due to crater lake overflow; and triggered primary volcanic activity.

Forced model response

Ensemble climate projection experiment data were obtained from the Coupled Model Intercomparison Project Phase 5 (CMIP5). We use data from nine separate models, listed in **Table 1**, each of which follow the Representative Concentration Pathway (RCP) 8.5 scenario. The total period covered by the selected data is from 2005 or 2006 to 2100. For comparability, we use models from ensemble r1i1p1 only, at a monthly frequency. For each model and each year over the modelled period, we calculate the mean global temperature $\langle T \rangle$ timeseries and the maximum monthly rainfall value RXm for each grid cell. The forced model response (FMR) is calculated as the slope of a linear regression of these parameters normalised to 01-Jan-2006 (Figures 1 and 2) or 01-Jan-2021 (**Figures 3** and **4**) . The resulting 2D array A_k, where k is the number of the model, has dimensions dependent on the initial spatial resolution of the model experiments (**Table 1**). For each model k, the value of each cell at latitude i and longitude j is binarised such that

$B_{ijk} = H(A_{ijk})$ where $H(x)$ is the Heaviside function and the boolean units 0 and 1 thus denote negative and positive forced model responses, respectively. To determine areas where the majority of models agree on the sign of heavy precipitation change, we resample the binary arrays onto a common grid using a nearest-neighbor approach, then sum them such that $C = \sum_{k=1}^{n=N} B_k$. Agreement in the sign of normalised RXm across at least seven of nine models is represented by $|C_{ij} - (9/2)| > 2$, where $C_{ij} \in [0,9]$. This criterion (7/9 models or 78 % model agreement) is comparable to the threshold imposed by previous studies[40,41].

Table 1| Nine CMIP5 models used in this study, including their spatial resolutions (number of mesh nodes).

Model	Modelling center	Spatial resolution
ACCESS1.3	CSIRO (Commonwealth Scientific and Industrial Research Organisation, Australia), and BOM (Bureau of Meteorology, Australia)	145 × 192
CNRM-CM5	Centre National de Recherches Météorologiques/Centre Européen de Recherche et Formation Avancées en Calcul Scientifique	128 × 256
CSIRO-Mk3.6.0	CSIRO (Commonwealth Scientific and Industrial Research Organisation, Australia), and BOM (Bureau of Meteorology, Australia)	96 × 192
CanESM2	Canadian Centre for Climate Modelling and Analysis	64 × 128
INM-CM4	Institute for Numerical Mathematics, Russia	120 × 180
IPSL-CM5A-MR	Institut Pierre-Simon Laplace, France	96 × 96
MIROC5	Atmosphere and Ocean Research Institute (The University of Tokyo), National Institute for Environmental Studies, and Japan Agency for Marine-Earth Science and Technology, Japan	128 × 256

MRI-CGCM3	Meteorological Research Institute, Japan	160 × 320
NorESM1-M	Norwegian Climate Centre, Norway	96 × 144

Distribution statistics and other calculations

Where appropriate, volcano slope steepness was calculated using the database compiled by ref. [44]. Based on Shuttle Radar Topography Mission (SRTM) digital elevation data, ref. [44] compute flank slopes for 50 m elevation intervals for 759 volcanoes. Maxima and mean slope values were calculated from this database. Uniformity was tested for using the chi-squared (χ^2) method. Statistical significance was ascribed where the cumulative distribution function of the chi-squared statistic CDF(χ^2) was less than 0.01. Descriptive statistics of volcano FMR distributions (**Figure 2c**) were calculated assuming a normal distribution ("negative" and "ambiguous") and a log-normal distribution ("positive"). All data processing and analysis was performed in Python 3. Links to all necessary code are provided in the Code Availability section.

References

1. Brönnimann, S. *et al.* Last phase of the Little Ice Age forced by volcanic eruptions. *Nat. Geosci.* **12**, 650–656 (2019).
2. Robock, A. Volcanic eruptions and climate. *Rev. Geophys.* **38**, 191–219 (2000).
3. Hyde, W. T. & Crowley, T. J. Probability of Future Climatically Significant Volcanic Eruptions. *J. Clim.* **13**, 1445–1450 (2000).
4. Bethke, I. *et al.* Potential volcanic impacts on future climate variability. *Nat. Clim. Change* **7**, 799–805 (2017).
5. Rampino, M. R., Self, S. & Fairbridge, R. W. Can Rapid Climatic Change Cause Volcanic Eruptions? *Science* **206**, 826–829 (1979).
6. Liggins, F., Betts, R. A. & McGuire, B. Projected future climate changes in the context of geological and geomorphological hazards. *Philos. Trans. R. Soc. Math. Phys. Eng. Sci.* **368**, 2347–2367 (2010).
7. Cooper, C. L., Swindles, G. T., Savov, I. P., Schmidt, A. & Bacon, K. L. Evaluating the relationship between climate change and volcanism. *Earth-Sci. Rev.* **177**, 238–247 (2018).
8. Albino, F., Pinel, V. & Sigmundsson, F. Influence of surface load variations on eruption likelihood: application to two Icelandic subglacial volcanoes, Grímsvötn and Katla. *Geophys. J. Int.* **181**, 1510–1524 (2010).
9. Swindles, G. T. *et al.* Climatic control on Icelandic volcanic activity during the mid-Holocene. *Geology* **46**, 47–50 (2017).

10. Bay, R. C., Bramall, N. & Price, P. B. Bipolar correlation of volcanism with millennial climate change. *Proc. Natl. Acad. Sci.* **101**, 6341–6345 (2004).
11. Capra, L. Abrupt climatic changes as triggering mechanisms of massive volcanic collapses. *J. Volcanol. Geotherm. Res.* **155**, 329–333 (2006).
12. McGuire, B. Potential for a hazardous geospheric response to projected future climate changes. *Philos. Trans. R. Soc. Math. Phys. Eng. Sci.* **368**, 2317–2345 (2010).
13. Mastin, L. G. Explosive tephra emissions at Mount St. Helens, 1989-1991: The violent escape of magmatic gas following storms? *GSA Bull.* **106**, 175–185 (1994).
14. Voight, B., Constantine, E. K., Siswowidjoyo, S. & Torley, R. Historical eruptions of Merapi Volcano, Central Java, Indonesia, 1768–1998. *J. Volcanol. Geotherm. Res.* **100**, 69–138 (2000).
15. McBirney, A. R. Thoughts on the eruption of the nicaraguan volcano las pilas. *Bull. Volcanol.* **17**, 113–117 (1955).
16. Matthews, A. J. *et al.* Rainfall-induced volcanic activity on Montserrat. *Geophys. Res. Lett.* **29**, 22-1-22–4 (2002).
17. Matthews, A. J. & Barclay, J. A thermodynamical model for rainfall-triggered volcanic dome collapse. *Geophys. Res. Lett.* **31**, (2004).
18. Hicks, P. D., Matthews, A. J. & Cooker, M. J. Triggering of a volcanic dome collapse by rainwater infiltration. *J. Geophys. Res.* **115**, B09212 (2010).
19. Barclay, J., Johnstone, J. E. & Matthews, A. J. Meteorological monitoring of an active volcano: Implications for eruption prediction. *J. Volcanol. Geotherm. Res.* **150**, 339–358 (2006).
20. Carn, S., Watts, R. B., Thompson, G. & Norton, G. E. Anatomy of a lava dome collapse: the 20 March 2000 event at Soufrière Hills Volcano, Montserrat. *J. Volcanol. Geotherm. Res.* **131**, 241–264 (2004).
21. Farquharson, J. I. & Amelung, F. Extreme rainfall triggered the 2018 rift eruption at Kīlauea Volcano. *Nature* **580**, 491–495 (2020).
22. McKee, C. O., Wallace, D. A., Almond, R. A. & Talai, B. Fatal hydro-eruption of Karkar volcano in 1979: Development of a maar-like crater. *Cooke-Ravian Vol. Volcanol. Pap. Geol. Surv. Papua N. Guin.* **10**, 63–84 (1981).
23. Global Volcanism Program. Report on Guagua Pichincha (Ecuador). *Bull. Glob. Volcanism Netw.* **18**, (1993).
24. Global Volcanism Program. Report on Karangetang [Api Siau] (Indonesia). *Bull. Glob. Volcanism Netw.* **36**, (2011).
25. Lagmay, A. M. F., Bagtasa, G., Crisologo, I. A., Racoma, B. A. B. & David, C. P. C. Volcanoes magnify Metro Manila's southwest monsoon rains and lethal floods. *Front. Earth Sci.* **2**, (2015).
26. Németh, K. & Kósik, S. Review of Explosive Hydrovolcanism. *Geosciences* **10**, 44 (2020).
27. Poulidis, A. P., Renfrew, I. A. & Matthews, A. J. Thermally Induced Convective Circulation and Precipitation over an Isolated Volcano. *J. Atmospheric Sci.* **73**, 1667–1686 (2016).
28. Paguican, E. M. R. *et al.* Extreme rainfall-induced lahars and dike breaching, 30 November 2006, Mayon Volcano, Philippines. *Bull. Volcanol.* **71**, 845–857 (2009).
29. Kataoka, K. S. *et al.* Lahar characteristics as a function of triggering mechanism at a seasonally snow-clad volcano: contrasting lahars following the 2014 phreatic eruption of Ontake Volcano, Japan. *Earth Planets Space* **70**, 113 (2018).

30. Baumann, V. *et al.* Mapping the susceptibility of rain-triggered lahars at Vulcano island (Italy) combining field characterization, geotechnical analysis, and numerical modelling. *Nat. Hazards Earth Syst. Sci.* **19**, 2421–2449 (2019).
31. Ayonghe, S. N., Ntasin, E. B., Samalang, P. & Suh, C. E. The June 27, 2001 landslide on volcanic cones in Limbe, Mount Cameroon, West Africa. *J. Afr. Earth Sci.* **39**, 435–439 (2004).
32. Marques, R., Zêzere, J., Trigo, R., Gaspar, J. & Trigo, I. Rainfall patterns and critical values associated with landslides in Povoação County (São Miguel Island, Azores): relationships with the North Atlantic Oscillation. *Hydrol. Process.* **22**, 478–494 (2008).
33. Towhata, I. *et al.* Mechanism and future risk of slope instability induced by extreme rainfall event in Izu Oshima Island, Japan. *Nat. Hazards* **105**, 501–530 (2021).
34. Eichenberger, J., Ferrari, A. & Laloui, L. Early warning thresholds for partially saturated slopes in volcanic ashes. *Comput. Geotech.* **49**, 79–89 (2013).
35. Manconi, A., Longpré, M.-A., Walter, T. R., Troll, V. R. & Hansteen, T. H. The effects of flank collapses on volcano plumbing systems. *Geology* **37**, 1099–1102 (2009).
36. Tebaldi, C., Hayhoe, K., Arblaster, J. M. & Meehl, G. A. Going to the Extremes. *Clim. Change* **79**, 185–211 (2006).
37. Min, S.-K., Zhang, X., Zwiers, F. W. & Hegerl, G. C. Human contribution to more-intense precipitation extremes. *Nature* **470**, 378–381 (2011).
38. Gu, G. & Adler, R. F. Spatial Patterns of Global Precipitation Change and Variability during 1901–2010. *J. Clim.* **28**, 4431–4453 (2015).
39. Collins, M. *et al.* Observational challenges in evaluating climate models. *Nat. Clim. Change* **3**, 940–941 (2013).
40. Fischer, E. M., Sedláček, J., Hawkins, E. & Knutti, R. Models agree on forced response pattern of precipitation and temperature extremes. *Geophys. Res. Lett.* **41**, 8554–8562 (2014).
41. Pfahl, S., O'Gorman, P. A. & Fischer, E. M. Understanding the regional pattern of projected future changes in extreme precipitation. *Nat. Clim. Change* **7**, 423–427 (2017).
42. Hürlimann, M., Ledesma, A. & Martí, J. Conditions favouring catastrophic landslides on Tenerife (Canary Islands). *Terra Nova* **11**, 106–111 (1999).
43. Hickson, C. Character of volcanism, volcanic hazards, and risk, northern end of the Cascade magmatic arc, British Columbia and Washington State. *Bull. - Geol. Surv. Can.* **481**, 231–250 (1994).
44. Grosse, P., Euillades, P. A., Euillades, L. D. & van Wyk de Vries, B. A global database of composite volcano morphometry. *Bull. Volcanol.* **76**, 784 (2013).
45. Deeming, K. R., McGuire, B. & Harrop, P. Climate forcing of volcano lateral collapse: evidence from Mount Etna, Sicily. *Philos. Trans. R. Soc. Math. Phys. Eng. Sci.* **368**, 2559–2577 (2010).
46. Jones, R., Manville, V., Peakall, J., Froude, M. J. & Odbert, H. M. Real-time prediction of rain-triggered lahars: incorporating seasonality and catchment recovery. *Nat. Hazards Earth Syst. Sci.* **17**, 2301–2312 (2017).
47. Scandone, R., Giacomelli, L. & Gasparini, P. Mount Vesuvius: 2000 years of volcanological observations. *J. Volcanol. Geotherm. Res.* **58**, 5–25 (1993).
48. Rolandi, G., Barrella, A. M. & Borrelli, A. The 1631 eruption of Vesuvius. *J. Volcanol. Geotherm. Res.* **58**, 183–201 (1993).
49. Hervás, J. Lessons Learnt from Landslide Disasters in Europe. in 102.

50. Lavigne, F., Thouret, J. C., Voight, B., Suwa, H. & Sumaryono, A. Lahars at Merapi volcano, Central Java: an overview. *J. Volcanol. Geotherm. Res.* **100**, 423–456 (2000).
51. Global Volcanism Program. Report on Fuego (Guatemala). *Sci. Event Alert Netw. Bull.* **12**, (1987).
52. Pierson, T. C., Wood, N. J. & Driedger, C. L. Reducing risk from lahar hazards: concepts, case studies, and roles for scientists. *J. Appl. Volcanol.* **3**, 16 (2014).
53. Nagatani, K. *et al.* Micro-unmanned aerial vehicle-based volcano observation system for debris flow evacuation warning. *J. Field Robot.* **35**, 1222–1241 (2018).
54. Sanderson, R. W., Matoza, R. S., Haymon, R. M., Steidl, J. H. & Hegarty, P. Lahar detection using infrasound: Pilot experiment at Mount Adams, WA. *AGU Fall Meet. Abstr.* **13**, (2018).
55. Global Volcanism Program. Report on Kirishimayama (Japan). *Bull. Glob. Volcanism Netw.* **36**, (2011).
56. McGuire, B. Climate forcing of geological and geomorphological hazards. *Philos. Trans. R. Soc. Math. Phys. Eng. Sci.* **368**, 2311–2315 (2010).
57. Impact of global warming on the rise of volcanic plumes and implications for future volcanic aerosol forcing - Aubry - 2016 - Journal of Geophysical Research: Atmospheres - Wiley Online Library. https://agupubs.onlinelibrary.wiley.com/doi/full/10.1002/2016JD025405.
58. Poulidis, A. P., Takemi, T., Iguchi, M. & Renfrew, I. A. Orographic effects on the transport and deposition of volcanic ash: A case study of Mount Sakurajima, Japan. *J. Geophys. Res. Atmospheres* **122**, 9332–9350 (2017).
59. Anderson, D. L. Earthquakes and the Rotation of the Earth. *Science* **186**, 49–50 (1974).
60. McGuire, W. J. *et al.* Correlation between rate of sea-level change and frequency of explosive volcanism in the Mediterranean. *Nature* **389**, 473–476 (1997).
61. Global Volcanism Program. *Volcanoes of the World, v. 4.9.1 (17 Sep 2020)*. https://doi.org/10.5479/si.GVP.VOTW4-2013 (2013).

Data Availability

Model output data have been obtained through Earth System Grid Federation servers, in particular the node hosted by the Lawrence Livermore National Laboratory (https://esgf-node.llnl.gov/search/cmip5/). Data generated in the present study are available at the following repository: TBC.

Code Availability

All necessary data and code required are provided in the following GitHub repository: https://github.com/jifarquharson/rainfall-in-volcanic-regions/tree/main/Projects/Climate_forcing. This includes links to relevant open access repositories from which data were accessed. Supplementary material is also provided in the following repository: TBC.

Author Contributions

FA and JF conceived the project. JF performed the data processing and analysis. Both authors contributed to writing the manuscript.

Conflicts of interest

The authors declare no conflicts of interest.

Acknowledgements

We thank the climate modelling groups listed in Table 1 for generating and making publicly available their model data. We also thank the attendant data distribution centers and the World Climate Research Programme’s Working Group on Coupled modelling, which is responsible for CMIP5. We also thank the Smithsonian Institution for developing and maintaining the Global Volcanism Program, from which data are openly available. We thank Sharanya Majumdar, Hannah Derbyshire, Fabian Wadsworth, and the WHWN writing group for invaluable discussions. This work was supported by funding from the NASA’s Interdisciplinary Research in Earth Science (IDS) program (grant number 80NSSC17K0028 P00003).